Vapor-phase isopropylation of phenol over Fe-containing Al-MCM-41 molecular sieves

R. Savidha,* A. Pandurangan, M. Palaichamy, and V. Murugesan

Department of Chemistry, Anna University, Chennai-600025, India

Received 6 June 2003; accepted 19 August 2003

Al-MCM-41 and Fe-containing MCM-41 molecular sieves are hydrothermally synthesized. The low-angle XRD analysis shows that iron incorporation in Al-MCM-41 retains the hexagonal structure of MCM-41. The higher *d*-spacing values of Fe-Al-MCM-41 catalysts than those of Al-MCM-41 indicate the incorporation of iron into the framework. The mesoporous nature of the materials was confirmed by nitrogen adsorption isotherms. Electron paramagnetic resonance (EPR) and diffuse reflectance spectra (DRS) techniques confirm the tetrahedral coordination of iron into the Al-MCM-41 framework. Acidity of the synthesized catalysts was analyzed by both TPD of ammonia and pyridine-adsorbed FT-IR spectroscopy. The acidity measurements indicate that iron incorporation increases both Lewis and Brønsted acidity of the catalysts. Vapor-phase isopropylation of phenol with the new alkylating agent isopropyl acetate was carried over the H-forms of the above catalysts. The phenol to isopropyl acetate ratio of 1 : 2 and the phenol space velocity of 1.1 h^{-1} were found to be the optimum conditions for better phenol conversion and para isomer (4-isopropyl phenol) selectivity. On comparison, the Fe-incorporated Al-MCM-41 catalysts show significantly higher phenol conversion and selectivity toward the important product 4-isopropyl phenol (4-IPP) may be due to stronger Brønsted acid sites generated by the strengthening effect of nearby Lewis acid sites. Further, the undesired and dialkylated products selectivity are found to be lower over Fe-incorporated Al-MCM-41 than pure Al-MCM-41 catalysts.

KEY WORDS: isopropylation; phenol; isopropyl acetate; Al-MCM-41; iron.

1. Introduction

Propylation of phenol is an important industrial reaction owing to the immense industrial importance of para isomers in the synthesis of a wide range of products such as adhesives, agricultural chemicals and pharmaceuticals [1]. Friedel–Crafts reaction is generally an acid-catalyzed reaction. A major emerging and challenging area of heterogeneous catalysis is that of environmental pollution control, with tightening legislation on the release of waste and toxic emissions having serious implications for the chemical industry. While heterogeneously catalyzed processes are widely used within the petrochemical industry, many fine and specialty chemical manufacturers rely on homogeneously catalyzed liquid-phase reactions. Many of these processes were developed at the turn of the century and focused in product yield, disregarding the environmental impact of inorganic waste and toxic by-products formed during the reaction. The problems associated with mineral acids and metal oxides as catalysts were minimized by the use of solid acid catalysts like zeolites and SAPOs. Reports are available in the literature for alkylation of aromatics over zeolites, and the product selectivity is found to depend on the acidic and basic nature of the catalysts and reaction temperature [2–4]. Venkat Rao *et al.* [5] studied the methylation of phenol over vanadia–chromia catalysts and found that acidic catalysts lead to preferential C-alkylation, forming 2,6-xylenol. The methylation of phenol over Y-zeolite studied by Namba *et al.* [6] revealed that alkylation at carbon and oxygen positions is competitive. Also, weakly acidic catalysts like (ultrastable) zeolite Y [7] lead to O-alkylated product as the major one, and strong acidic catalysts like zeolite-β [8] or a high reaction temperature produces C-alkylated products, particularly *m*-isomer. The moderately acidic catalysts such as ZSM-12 [9], zeolite Y [10] and SAPO-11 [11] are considered suitable for the formation of the para isomer in phenol alkylation.

Zhang *et al.* [12] studied the *t*-butylation of phenol with *t*-butanol over zeolite H-β and found that strong acid sites are helpful for the formation of 2,4-DTBP and medium acid sites are advantageous to produce *p*-isomer (*p*-TBP), while weak acid sites are effective in producing the ortho isomers. Yoo *et al.* [13] carried out isopropylation of phenol with 2-propanol over Na-exchanged ZSM-5 and reported that isopropylation takes place exclusively at carbon centers. Further, they reported that the phenol conversion and products selectivity (except 4IPP) remains constant with increasing sodium ion exchange. The phenol conversion decreased with increasing sodium ion exchange because of the reduction of number of acid sites by the Na^+ ions. However, the use of zeolites and SAPOs for alkylation of larger molecules is limited because of the available pore

* To whom correspondence should be addressed.
E-mail: savidha@hotmail.com

1011-372X/03/1100–0049/0

dimensions and rapid deactivation by impurities. The limitation of restricted pore size has been overcome by the discovery of MCM-41, which possess hexagonal mesopores, high surface area and tunable pore size and acidity [14,15]. The incorporation of trivalent cations like aluminum, chromium, vanadium, titanium and boron into the MCM-41 framework has been found to generate additional moderate to strong acidity and hence catalytic activity [16–19]. Sakthivel *et al*. [20] carried out *t*-butylation of phenol over H-Al-MCM-41 and observed higher substrate conversion and para-selectivity than that over zeolites and SAPOs and accounted in terms of moderate to strong acidity, large surface area and the mesoporous nature of the H-Al-MCM-41. He *et al*. [21] reported that Fe-MCM-41 molecular sieves are very active in benzylation of benzene with 100% monoalkylation selectivity and better stability. Also, Badamali *et al*. [22] carried out *t*-butylation of phenol over H-Fe-MCM-41 and observed *p*-*t*-butyl phenol as the major product with high selectivity.

Hence, in the present study, it is proposed to incorporate the transition metal iron in Al-MCM-41 framework to generate additional moderate to strong acid sites on Al-MCM-41 and to carry out the isopropylation of phenol with isopropyl acetate, a new alkylating agent. In conventional methods, propylene and isopropyl alcohol has been used as the alkylating agent. These reagents possess some demerits as the former could deactivate the catalyst by yielding polybutenes (oligomerization), and the latter, isopropyl alcohol, although could discourage the coke formation, would get aggregated near Brønsted acid sites through hydrogen bonding, thereby suppressing dissociation. Isopropyl acetate has many advantages over the conventional reagents, as it could get better adsorbed on the Brønsted acid sites. It may be due to the easy availability of free active site of adsorption, namely, the carbonyl group of IPA, compared to the sterically crowded alcoholic OH in isopropyl alcohol. To our knowledge, no report is available in the literature on the isopropylation of phenol using isopropyl acetate as the alkylating agent. Further, conditions were optimized in order to attain higher substrate conversion and selectivity toward *para*-isopropyl phenol, a commercially important product.

2. Experimental

2.1. Chemicals

All the reagents, viz., sodium metasilicate, aluminum sulfate, ferric nitrate, cetyl trimethyl ammonium bromide (CTAB), sulfuric acid, isopropyl acetate and phenol were of AR grade purchased from E-merck India Ltd.

2.1.1. Synthesis of catalytic materials

Al-MCM-41(Si/Al = 100 and 50) samples were synthesized hydrothermally using a gel composition of $SiO_2 : xAl_2O_3 : 0.2CTAB : 0.89H_2SO_4 : 120H_2O$ (x = varies with Si/Al ratio). Sodium metasilicate and aluminum sulfate were used as the sources for silicon and aluminum respectively. Cetyl trimethyl ammonium bromide (CTAB) was used as the structure-directing agent. In a typical synthesis, 10.6 g of sodium metasilicate in water was combined with appropriate amount of aluminum sulfate in distilled water and the pH of the solution was adjusted to 10.5 with constant stirring to form a gel. After 30 min, an aqueous solution of CTAB was added to it and the mixture was stirred for 1 h at room temperature. The suspension was then transferred into a 300-mL stainless steel autoclave, sealed and heated in a hot air oven at 160 °C for 48 h. After cooling to room temperature, the product formed was filtered, washed with deionized water and dried. Using ferric nitrate as the source for iron, Fe-Al-MCM-41 (Si/Fe = 100 and 50) was prepared hydrothermally. The dried materials were calcined at 550 °C for 1 h in nitrogen atmosphere followed by 5 h in air. In Fe-Al-MCM-41 catalysts, the Si/Al ratio was kept 100. The calcined materials were converted into H-form by repeated ion exchange with aqueous 1 M NH_4Cl solution followed by calcination at 550 °C for 6 h.

2.2. Characterization

2.2.1. XRD

The low-angle X-ray powder diffractograms of calcined Al-MCM-41 and Fe-Al-MCM-41 samples were obtained on a Philips PW1050 diffractometer equipped with liquid nitrogen-cooled germanium solid-state detector using Cu Kα radiation. The samples were scanned from 1 to 10° (2θ) in steps of 0.02 with the counting time of 5 s at each point.

2.2.2. Textural properties

The surface area measurements of all the catalyst samples were carried out by nitrogen adsorption at 77 K in an ASAP-2010 volumetric adsorption analyzer manufactured by Micromeritics Corporation (Norcross, Ga). Before the nitrogen adsorption–desorption measurements, each sample was degassed at 623 K at 10^{-5} torr. The specific areas of the samples were determined from the linear part of the BET plots. The pore-size distribution was calculated from the nitrogen adsorption–desorption isotherms using the BJH algorithm (ASAP201 built-in software from Micromeritics). Chemical analysis was performed with an ICP-AES Labtum plasma 8440 instrument. The silica content was determined after dissolution with HF, and the alumina content was determined after dissolution with borax.

2.2.3. SEM

The size and morphology of Al-MCM-41 (50) and Fe-Al-MCM-41 (50) samples were examined by scanning electron microscopy using JEOL 640 instrument. Samples were gold coated using an Instrumental Scientific Instruments PS-2 coating unit. The SEM pictures are developed using thin photographic paper.

2.2.4. ^{27}Al MAS NMR

Solid-state ^{27}AlMASNMR measurements for Al-MCM-41 (50) and Fe-Al-MCM-41 (50) were performed on an MSL 400 spectrometer equipped with a magic angle-spinning (MAS) unit. The ^{27}Al MAS NMR spectra were recorded at a frequency of 104.22 MHz and at a spinning rate of 8 KHz with a pulse length of 1.0 μs, a delay time of 0.2 s, a spectral width of 330 ppm and 150 scans. The line broadening was 50 Hz. The ^{27}Al chemical shifts were reported in relation to the liquid solution of aluminum nitrate.

2.2.5. DRS

The coordination environment of iron in Fe-Al-MCM-41 samples was examined by diffuse reflectance UV–vis spectroscopy. The spectra were recorded in Shimadzu, (UV–vis spectrophotometer Model 2101 PC) in the wavelength range of 200 to 600 nm.

2.2.6. EPR

The coordination environment of iron in Fe-Al-MCM-41 (50 and 100) samples was further confirmed by electron paramagnetic resonance (EPR) analysis recorded on a JEOL EPR spectrometer (JES-RE1XM) operating in the X-band region. The microwave power employed was 3.0 mW, and the amplitude of magnetic field modulation at 100 kHz was 0.03 mT. All observations were made at room temperature. 40 mg of the sample was taken in a quartz tube with 4-mm o.d., evacuated to $\approx 10^{-3}$ torr. The tube was sealed under vacuum and then set in the quartz Dewar vessel fitted in the EPR cavity. DPPH ($g = 2.0037$) was used as a reference to mark the g-value.

2.3. Acidity measurements

2.3.1. TPD of Ammonia

The acidity of Al-MCM-41 and substituted Al-MCM-41 samples was analyzed by both TPD of NH_3 by TGA method as well as pyridine-adsorbed FT-TR spectroscopy. Adsorption of ammonia was carried out on each sample in a quartz tube packed with 0.5 g of the catalyst. Initial flushing was carried out with dry nitrogen for 3 h. Then, the system was evacuated (1.5×10^{-5} torr) at 550 °C for 5 h and cooled to room temperature. Ammonia adsorption was carried out by passing the ammonia vapors over the catalyst bed. After adsorption, the system was evacuated to remove the physisorbed ammonia and again ammonia was passed through the system. The adsorption and evacuation processes were repeated five times for saturating the molecular sieves. The extent of ammonia adsorbed over each catalyst was measured by TGA in a TA 3000 Mettler system. Nitrogen as purge gas was passed during desorption of ammonia. The TGA study was conducted at a heating rate of 10 °C/min up to 600 °C.

2.3.2. Pyridine-adsorbed FT-IR spectroscopy

Finely ground catalyst sample (10^{-15} mg) was pressed into a self-supporting wafer 13 mm in diameter. The wafers were calcined under vacuum (10^{-3} torr, 1 torr = 133.3 N/m^2) at 500 °C for 2 h, followed by exposure to pyridine vapor at ambient temperature and heating at 100 °C for 1 h to allow the pyridine to permeate the samples. The wafers were then allowed to cool to ambient temperature and evacuated for 1 h. The thin wafer was placed in the FT-IR cell and the spectrum was recorded in absorbance mode on a Nicolet 800 (AVATAR) FT-IR spectrometer, fully controlled by the OMNIC software, and an all-glass high-vacuum system.

2.4. Catalytic studies

The isopropylation of phenol with isopropyl acetate was carried out in a fixed-bed down-flow quartz reactor under atmospheric pressure in the temperature range of 250 to 400 °C in steps of 50 °C. Prior to the reaction, the reactor packed with 0.5 g of the catalyst sample was preheated in a tubular furnace equipped with a thermocouple. A mixture of phenol and isopropyl acetate was fed into the reactor using a syringe infusion pump at a predetermined flow rate. The isopropylation reaction was carried out, and the product mixture was collected for a time interval of 1 h. The products were analyzed by gas chromatography (Hewlett Packard 5890A) equipped with a flame ionization detector and an SE-30 column. The identification of products was facilitated by GC-MS (Perkin Elmer Elite series PE-5, capillary column, 30 m $\times$ 0.25 mm $\times$ 1 μm). The material balance calculation shows that more than 95% of the reactants were recovered as products.

3. Results and discussion

3.1. XRD

The purity and structure of the synthesized materials were analyzed by the low-angle XRD. The low-angle XRD patterns of calcined Al-MCM-41 (50) and Fe-Al-MCM-41 (50) samples are shown in figure 1. It can be observed that all the above materials exhibit a strong peak in the 2θ range 1.8 to 2.2° due to 100 plane reflection lines and small peaks due to higher order 110,

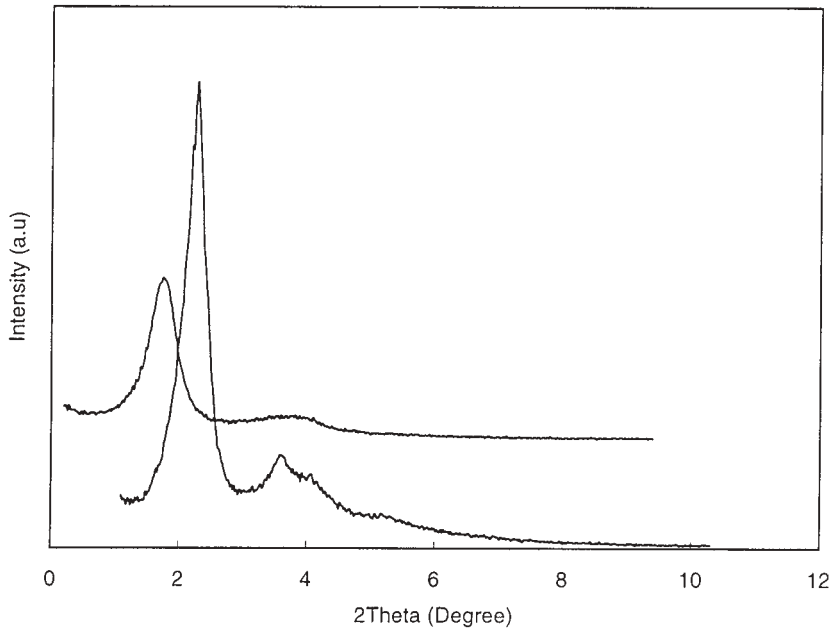

Figure 1. Low-angle XRD patterns of (a) Al-MCM-41 (50) and (b) Fe-Al-MCM-41 (50) catalysts.

200 and 210 plane reflections, indicating the formation of well-ordered mesoporous materials. These peaks are generally indexed to the hexagonal regularity of MCM-41. It is observed that the XRD patterns obtained are found to be in good agreement with previous reports for similar materials [23]. Further, the appearance of the above peaks in Fe-Al-MCM-41 (50) catalyst suggests that the hexagonal array of mesopores in MCM-41 was sustained after the incorporation of iron in the framework. The reduction in peak intensity and broadening of (100) peak of Fe-Al-MCM-41 sample compared with that of Al-MCM-41 is the indication of slight reduction in hexagonal symmetry of MCM-41 due to iron incorporation. In the case of Fe-Al-MCM-41, the *d*-spacing and hence the unit cell parameters (a_0) calculated from $2d(100)/\sqrt{3}$ is found to be larger compared with that of pure Al-MCM-41 [24]. The *d*-spacing value of Al-MCM-41 (50) is 38.4 Å and that of Fe-Al-MCM-41 (50) is 46.5 Å. The enlargement in the unit cell parameter of Fe-substituted materials is an expected one since the incorporation of metal cations with ionic radius larger than Si^{4+} and Al^{3+} leads to larger M–O bond distance. The ionic radius of Fe^{3+} (74 pm) is larger than that of Si^{4+} (40 pm) or Al^{3+} (53 pm); the increase in *d*-spacing is the indication of the incorporation of iron ions into the Al-MCM-41 framework.

3.1.1. BET surface area

The nitrogen adsorption isotherms were obtained for the above catalysts, and the typical isotherm for the model catalysts Al-MCM-41 (50) and Fe-Al-MCM-41 (50) is presented in figures 2(a) and (b) respectively. It is observed that there are three different well-defined stages in the isotherms. The initial increase in nitrogen uptake at low P/P_0 may be due to monolayer adsorption on the pore walls, a sharp step at intermediate P/P_0 may indicate the capillary condensation in the mesopores and a plateau portion at higher P/P_0 associated with multilayer adsorption on the external surface of the materials. All the catalysts show a characteristic step around the $P/P_0 \approx 0.4$, indicating the mesoporous nature of the materials [25]. The sharpness and height of the capillary condensation step are the indications of pore-size uniformity. Deviations from sharp and well-defined pore-filling step are the indications of increase in pore-size heterogeneity. The Al-MCM-41 samples exhibit isotherm with well-developed step in the relative pressure range ≈ 0.42, characteristic of capillary condensation into uniform mesopores. The incorporation of iron in the Al-MCM-41 framework is found to lower the P/P_0 for capillary condensation step. The pore diameter and pore volume is found to decrease with increasing metal (Al and Fe) incorporation over all the catalysts. Also, all the samples have high BET surface area (929–844 m^2/g), which is characteristic of mesoporous materials. Table 1 shows the detailed physicochemical characteristics of all the catalytic materials.

3.1.2. SEM

The size and morphology of Al-MCM-41 (50) and Fe-Al-MCM-41 (50) were investigated by scanning electron microscopy. The SEM pictures of these catalysts are presented in figures 3(a) and (b) respectively. All the samples do not have well-defined

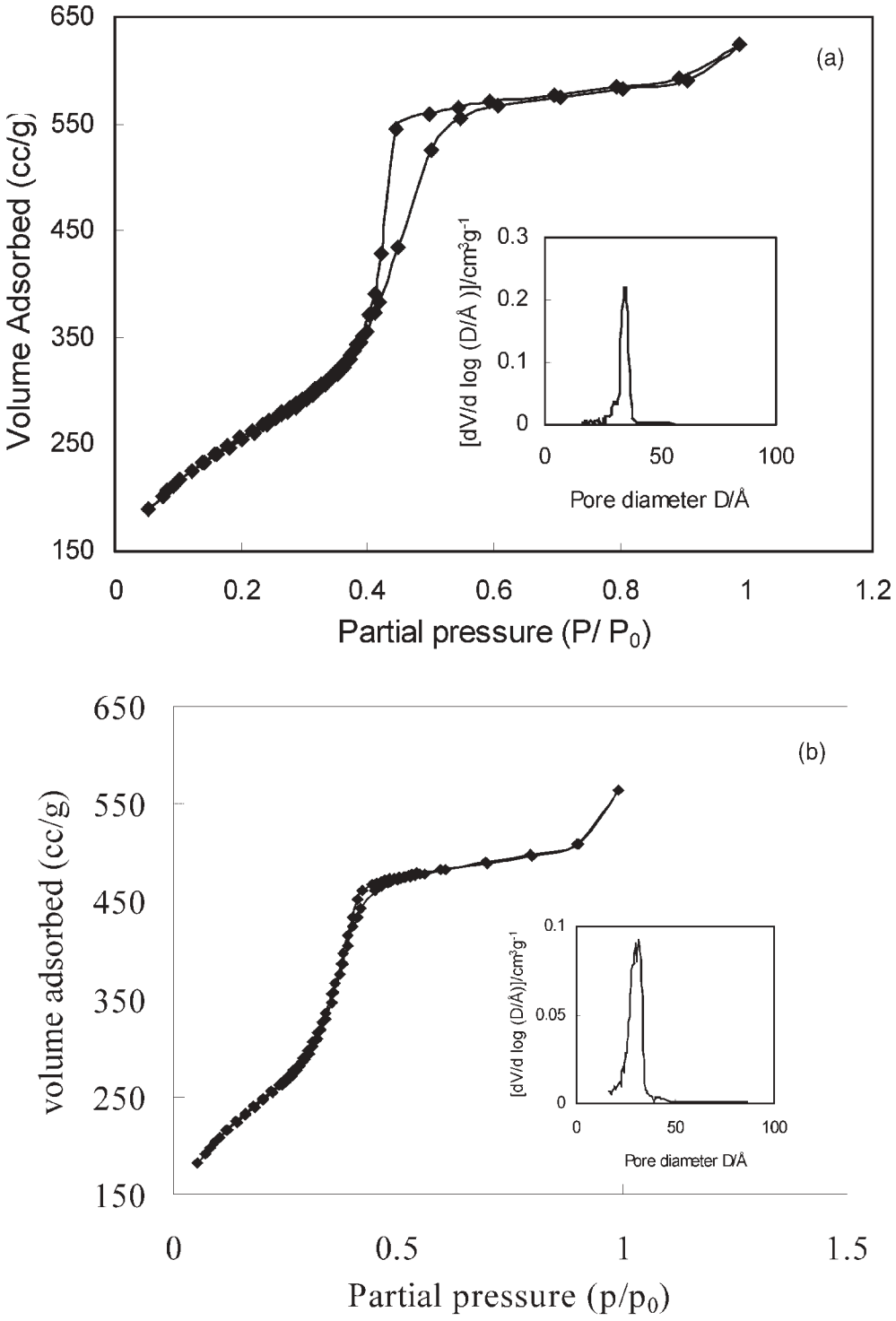

Figure 2. Nitrogen adsorption isotherm of (a) Al-MCM-41 (50) and (b) Fe-Al-MCM-41 (50) catalysts.

hexagonal structure. Further, aggregates without regular shapes are observed in agreement with previous reports [26] for metal-incorporated materials.

3.1.3. ^{27}Al MAS NMR

The incorporation of aluminum into the framework of Al-MCM-41 (50) and Fe-Al-MCM-41 (50) samples was analyzed by ^{27}Al MAS NMR spectroscopy, and the spectra of as-synthesized and calcined forms of all catalysts are presented in figures 4(a) and (b) respectively. The spectra of the as-synthesized and calcined samples show a sharp resonance peak from tetrahedrally coordinated aluminum at $\delta = 53.2$ and 53.7 ppm respectively, indicating that the aluminum is incorporated into the framework [27]. No peak at 0 ppm corresponding to octahedral aluminum species is observed in the case of

Table 1
Physicochemical characteristics of pure and Fe-incorporated Al-MCM-41 catalysts

Catalyst	Si/M* ratio		*d*-spacing (Å)	BET surface area (m^2/g)	Pore diameter (Å)	Pore volume (cm^3/g)	TPD of NH_3		Total acidity (mmol/g)
	Initial gel	Calcined[a]					LT-peak	HT-peak	
Al-MCM-41	100	107	36.5	929	34.7	0.99	0.175	0.120	0.295
Al-MCM-41	50	52	38.4	893	33.9	0.93	0.210	0.127	0.337
Fe-Al-MCM-41	100	98.3	45.5	853	30.9	0.88	0.282	0.157	0.439
Fe-Al-MCM-41	50	61.5	46.5	844	30.1	0.83	0.310	0.185	0.495

as-synthesized samples. But in the case of calcined samples, the appearance of a broad low intensity peak at $\delta = 0.6$ ppm indicates the presence of octahedral aluminum. The appearance of octahedral aluminum in calcined samples indicates that during the course of calcination some aluminum species are removed from the framework. The ^{27}Al signals are found to be broader than the signals generally observed for zeolitic aluminum, presumably because of the presence of greater distortions in the tetrahedral environment [28].

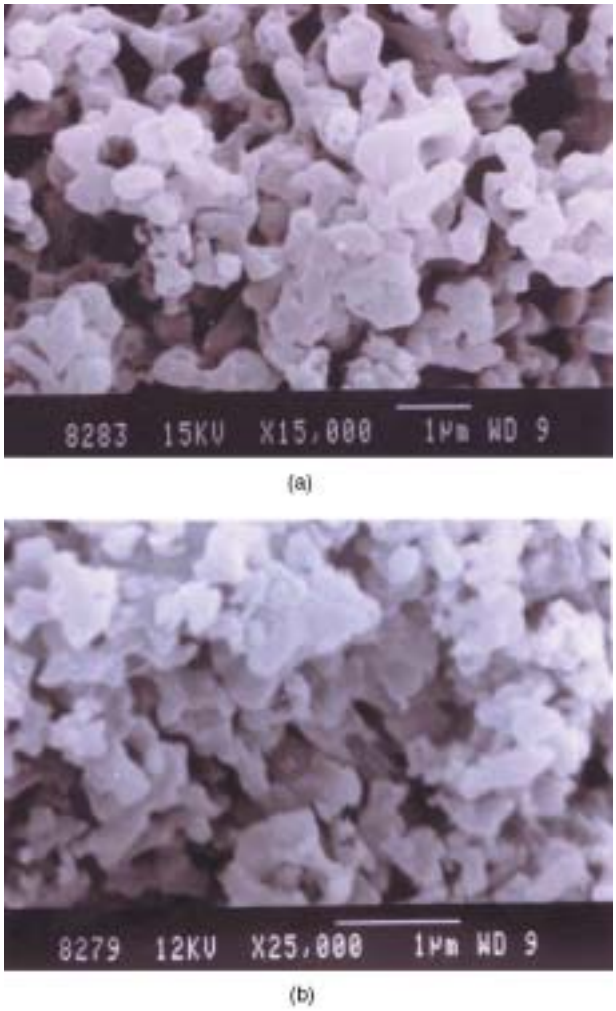

Figure 3. SEM pictures of (a) Al-MCM-41 (50) and (b) Fe-Al-MCM-41 (50) catalysts.

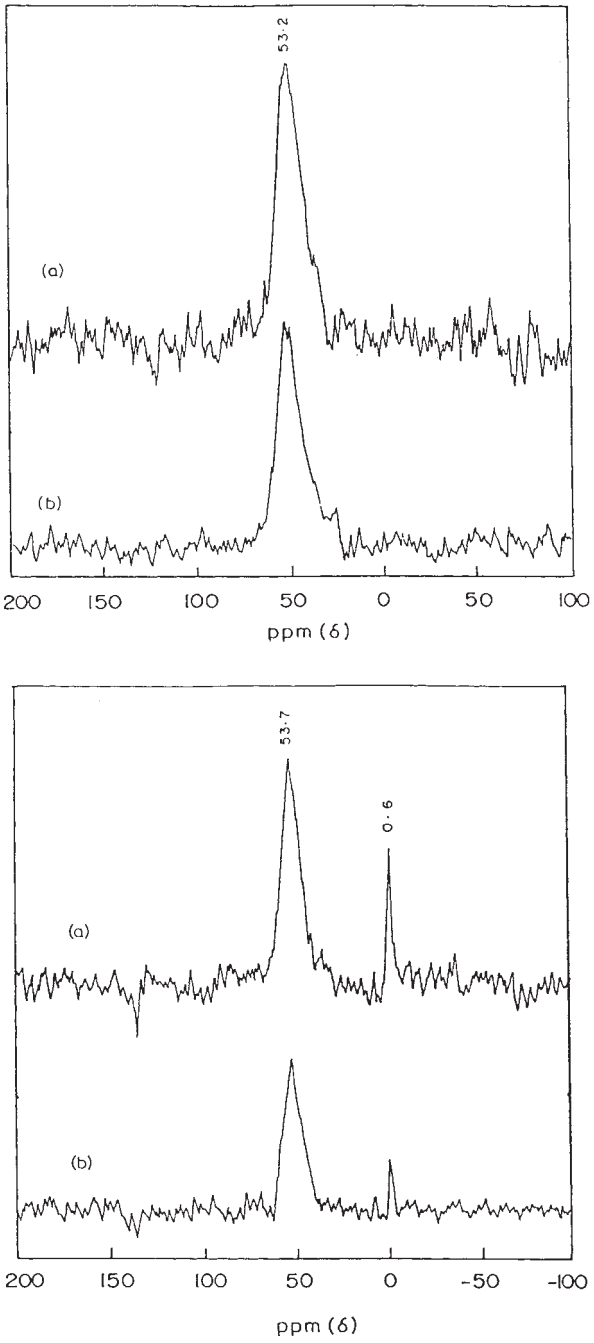

Figure 4. ^{27}Al MAS NMR spectra of (a) as-synthesized (b) calcined catalysts (a) Al-MCM-41 (50) and (b) Fe-Al-MCM-41 (50).

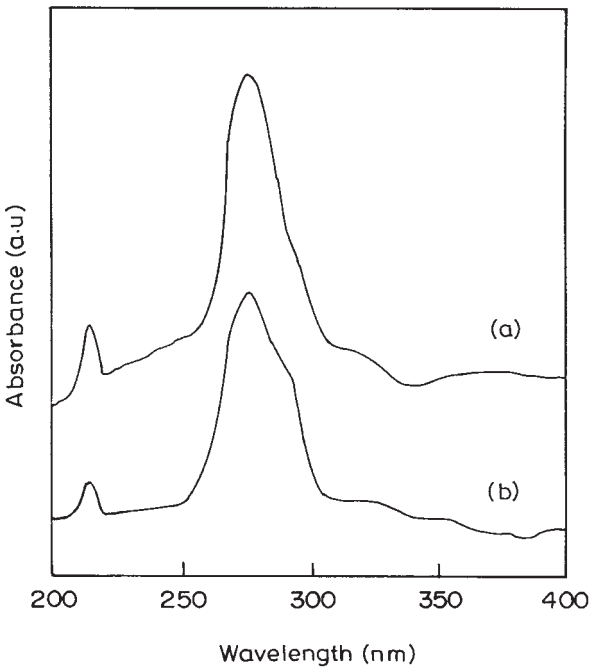

Figure 5. Diffuse reflectance UV–vis spectra of calcined Fe-Al-MCM-41 catalysts (a) Fe-Al-MCM-41 (50), (b) Fe-Al-MCM-41 (100).

3.1.4. DRS

The diffuse reflectance UV–vis spectra were recorded for calcined Fe-Al-MCM-41 catalysts in order to study the coordination environment of iron, and the spectra are shown in figure 5. A broad peak around 275 nm, which is similar to that of ferrisilicate containing tetrahedrally coordinated iron species was observed over both Fe-Al-MCM-41 catalysts. This band could be assigned to the $d\pi$-$p\pi$ charge transfer between the iron and oxygen atoms in the framework of Fe-O-Si in the zeolite [29]. A small peak around 215 nm may be due to octahedrally coordinated iron. Also, the as-synthesized samples exhibited white color, suggesting that no bulk iron oxide existed, and all the iron cations were probably incorporated inside the framework after the hydrothermal synthesis. After calcinations, the samples become off-white in color, possibly suggesting the presence of the extra framework iron.

3.1.5. EPR

The coordination environment of iron is further analyzed by EPR spectroscopy. The EPR spectrum of calcined Fe-Al-MCM-41 catalysts is shown in figure 6. Two signals at $g = 2.1$ and 4.25 were mainly detected. The signal at $g = 4.25$ could be attributed to Fe (III) ion in tetrahedral coordination with strong rhombic distortion [30]. The small shoulder at $g = 2.1$ can be attributed to Fe (III) in octahedral coordination [31,32].

3.1.6. Acidity measurements

3.1.6.1. TPD of NH_3

The total acidity of all the catalytic materials was measured by TPD of ammonia by the TGA method.

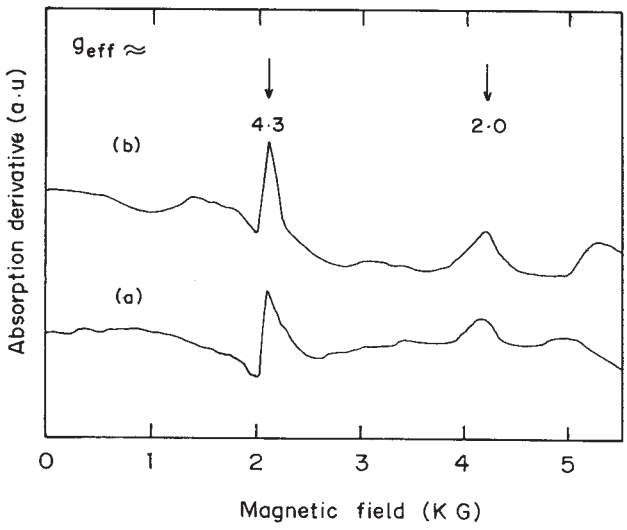

Figure 6. EPR spectra of calcined Fe-Al-MCM-41 catalysts (a) Fe-Al-MCM-41 (50), (b) Fe-Al-MCM-41 (100).

The desorption temperature and the amount of ammonia desorbed are considered as indexes of acid strength and total number of acid sites respectively. The amount of ammonia desorbed and desorption temperature of all the catalytic materials are presented in table 1. It is observed that two major weight losses occurred over all the catalysts at lower and higher temperature ranges. They may be due to desorption of adsorbed ammonia on weak and strong acid sites. The first and second weight losses occurred between 200 and 225 °C and 385 and 420 °C respectively for all the catalytic systems [33]. No significant change in desorption temperature is observed due to iron incorporation in Al-MCM-41. But the amount of ammonia desorbed at both the lower and the higher temperature range is found to increase on iron incorporation and increases with increasing iron content. Fe-Al-MCM-41(50) shows the total acidity of 0.495 mmol/g which is slightly higher than that of catalyst A1-MCM-41 (50) (0.337 mmol/g).

3.1.6.2. Pyridine-adsorbed FT-IR spectroscopy

The pyridine-adsorbed FT-IR spectra for catalysts Al-MCM-41 (50) and Fe-Al-MCM-41 (50) were recorded and presented in figure 7. It is observed that all the catalytic systems claim the presence of both Brønsted and Lewis acid sites. Typically, a sharp peak appeared at 1545 cm^{-1}, which is the indication of pyridine adsorbed on Brønsted acid sites. A small peak at 1455 cm^{-1} and a high intensity peak around 1620 cm^{-1} indicated the pyridine adsorbed on Lewis acid sites. A broad peak that appeared around 1500 cm^{-1} is the combination band of Brønsted and Lewis acid sites [34,35]. It is interesting to note that the intensity of both Lewis and Brønsted acid site peaks are found to be higher for Fe-Al-MCM-41 (50) catalyst than that of Al-MCM-41 (50), i.e., the incorporation of iron in Al-MCM-41 framework increases the number of

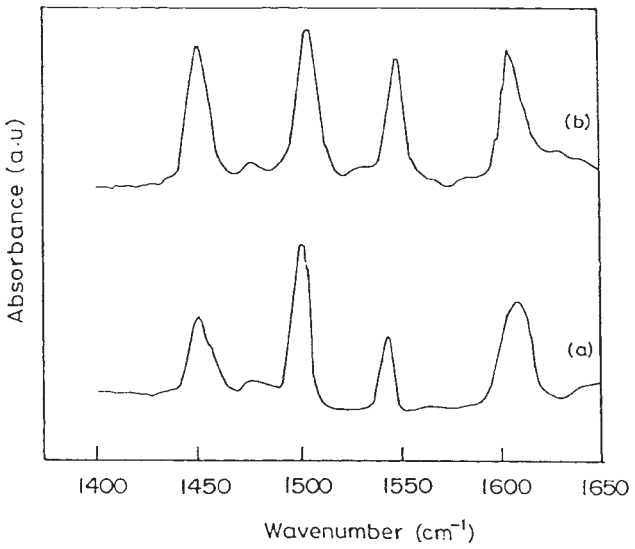

Figure 7. Pyridine-adsorbed FT-IR spectra of (a) Al-MCM-41 (50) and (b) Fe-Al-MCM-41 (50) catalysts.

both Brønsted and Lewis acid sites of the resulting material, similar to the observation made in TPD of ammonia. The iron incorporation in Al-MCM-41 is found to generate additional acidity.

3.2. Catalytic studies

Isopropylation of phenol with isopropyl acetate was carried out over the H-form of Al-MCM-41 and Fe-Al-MCM-41 catalysts in the temperature range of 250 to 400 °C in steps of 50 °C. The optimized molar ratio of phenol to isopropyl acetate (1 : 2) and phenol space velocity (LHSV = 1.1 h^{-1}) were used for all the catalytic runs. Product analysis shows that 4-isopropyl phenol (4-IPP), 2-isopropyl phenol (2-IPP), 2,4-diisopropyl phenol (2,4-DIPP), 2,6–diisopropyl phenol (2,6-DIPP) and isopropyl phenyl ether (IPPE) are the major products along with small amounts of undesired cracked and oligomerized products. The formation of the above products indicates that isopropylation occurs at carbon and the oxygen sites of phenol. However, the extent of the latter is small compared to that of the former.

3.2.1. Effect of feed molar ratio

Isopropylation of phenol with isopropyl acetate was carried out at 300 °C over H-form of Al-MCM-41 (50) and Fe-Al-MCM-41 (50) catalysts with varying (2 : 1, 1 : 1, 1 : 2 and 1 : 3) phenol to IPA molar ratio at the phenol space velocity of 1.1 h^{-1} in order to study the effect of feed ratio on phenol conversion and products selectivity. The products distribution at various molar feed ratios is presented in table 2. It is observed that the phenol conversion is found to increase with decreasing phenol content in the feed (increasing IPA content). When decreasing the phenol to IPA molar ratio from 2 : 1 to 1 : 3, the phenol conversion is found to increase from 34.8 to 47.0 wt% over Al-MCM-41 (50). Similarly, over catalyst Fe-Al-MCM-41 (50), the corresponding conversions are 49.7 and 63.5 wt% respectively. It is clear from table 2 that a decrease in phenol to IPA ratio increases the phenol conversion. It can be accounted that isopropyl acetate may compete with phenol for the adsorption sites, and with increasing molar excess of alkylating agent, the phenol conversion increases similar to other reports [12,20]. Also, the selectivity of 2-IPP and diisopropyl phenols (2,4-DIPP + 2,6-DIPP) are found to increase with decreasing the phenol to IPA ratio from 2 : 1 to 1 : 3. The selectivities of 2-IPP and DIPPs over Al-MCM-41 (50) are increased from 20.0 and 24.7% to 29.7 and 35.7% respectively. A similar trend is observed over the Fe-Al-MCM-41 (50) system. In contrast, the selectivity of 4-IPP is found to decrease with increasing IPA (decreasing phenol content) in the feed. Catalyst Al-MCM-41 (50) shows the 4-IPP selectivity of 47.1% at the feed ratio of 2 : 1 and the same is decreased to 20.4%, when the feed ratio is changed to 1 : 3. The decrease in 4-IPP selectivity is marginal up to the feed ratio of 1 : 2, and drastic thereafter. The 4-IPP selectivity over Al-MCM-41(50) and Fe-Al-MCM-41 (50) catalysts are 32.75 and 36.9%

Table 2
Effect of feed molar ratio and phenol space velocity on the product distribution over different catalysts at 300 °C

Feed ratio Phenol : isopropyl acetate	Al-MCM-41 (50)					Fe-Al-MCM-41 (50)				
	*Conv.	4-IPP	2-IPP	DIPP	Others	*Conv.	4-IPP	2-IPP	DIPP	Others
2 : 1	34.8	47.1	20.1	24.7	8.0	49.7	49.1	17.1	27.2	6.6
1 : 1	40.5	37.0	24.0	29.1	9.9	54.5	40.0	21.5	30.3	8.2
1 : 2	46.4	32.8	25.9	29.5	11.8	62.2	37.0	23.3	26.5	13.2
1 : 3	47.0	20.4	29.8	35.7	14.0	63.5	27.6	26.5	33.0	12.9
LHSV (h^{-1})										
0.55	47.5	33.7	29.5	27.8	9.0	65.5	33.1	29.0	26.7	11.2
1.1	46.4	32.8	25.9	29.5	11.8	62.2	33.8	26.5	26.5	13.2
1.65	37.8	19.8	22.0	45.5	12.7	51.3	29.3	25.3	31.8	13.6
2.2	26.5	18.9	15.4	47.2	18.5	34.5	26.1	24.6	34.8	14.5

Note: Weight of catalyst: 0.5 g, time onstream = 1 h.

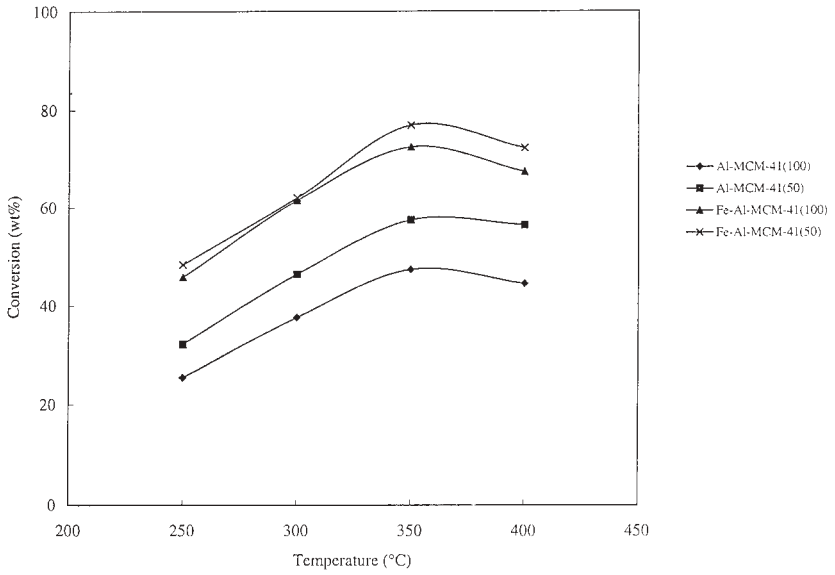

Figure 8. Effect of temperature on phenol conversion over various catalysts.

and 20.4 and 27.5% respectively at the phenol to IPA ratio of 1 : 2 and 1 : 3 respectively. The increase in DIPPs selectivity with increasing IPA content may be due to the higher concentration of IPA, which leads to dialkylation or polyalkylation. At lower phenol to IPA ratio (1 : 3), the selectivity of 4-IPP is found to decrease drastically with increasing undesired products including IPPE. Considering the phenol conversion and 4-IPP selectivity, the optimum phenol to IPA ratio of 1 : 2 was followed for further studies.

3.2.2. *Effect of phenol space velocity (LHSV)*

The products distribution obtained in isopropylation of phenol at 300 °C over Al-MCM-41 (50) and Fe-Al-MCM-41 (50) at different phenol space velocities (0.55, 1.1, 1.65 and 2.2 h^{-1}) are presented in table 2. It is observed that there is no significant change in phenol conversion, when the space velocity (LHSV) is increased from 0.55 to 1.1 h^{-1} over both the catalysts. Catalyst Al-MCM-41 (50) shows 47.5 wt% phenol conversion at LHSV = 0.55 h^{-1} and when LHSV is increased to 1.1 h^{-1}, the phenol conversion is around 46.4 wt%. Further increase in space velocity of phenol leads to the decrease in phenol conversion drastically. The phenol conversion is decreased to 26.0 wt% from 46.4 wt% when the phenol space velocity is increased to 2.2 h^{-1} from 1.1 h^{-1} over Al-MCM-41 (50). The low phenol conversion at higher space velocities can be accounted in terms of the shorter contact time at higher space velocities of phenol. Also, the selectivity of 4-IPP and 2-IPP is found to decrease with decreasing phenol space velocity. The fall in 4-IPP selectivity is found to be low up to the phenol space velocity (LHSV) of 1.1 h^{-1} and further increase in phenol space velocity leads to a drastic fall in 4-IPP selectivity. A similar trend is observed over all other catalysts. But the selectivity of DIPPs (2,4-DIPP and 2,6-DIPP) is found to increase with decreasing phenol space velocity, which may be due to polyalkylation, enhanced by longer contact time and more availability of free alkylating agent. Considering the phenol conversion as well as *p*-isomer (4-IPP) selectivity, the phenol space velocity of 1.1 h^{-1} was chosen as the optimum for further studies.

3.2.3. *Effect of reaction temperature*

Isopropylation of phenol was carried out over the H-form of catalysts Al-MCM-41 (100 and 50) and Fe-MCM-41 (100 and 50) in the temperature range of 250 to 400 °C in steps of 50 °C. The optimized phenol to IPA molar ratio (1 : 2) and phenol space velocity (1.1 h^{-1}) were followed for all the catalytic runs. The phenol conversion at various reaction temperatures over all the above catalytic systems is presented in figure 8, and the product distribution is presented in table 3. The phenol conversion is found to increase steadily with increasing reaction temperature up to 350 °C over all the catalytic systems. Further increase in temperature leads to a slight fall in conversion over all the catalytic systems. The decrease in phenol conversion at higher temperatures could be due to simultaneous deisopropylation of the product isopropyl phenol into phenol and lower hydrocarbons. At higher reaction temperatures, the formation of undesired products was enhanced. The formed undesired products may consume the reactant (IPA) without producing desired products and might lead to lower phenol conversion. Similar results were already reported for *t*-butylation of phenol over H-β catalysts by Zhang *et al*. [12]. In the case of Al-MCM-41 catalysts, the increase in aluminum content (decreasing Si/Al ratio) as well as total acidity is found to increase the phenol conversion at all the temperatures studied. At 350 °C, the Al-MCM-41 with Si/Al ratio of 100 and 50

Table 3
Products distribution of phenol isopropylation over different catalysts at different reaction temperatures

	250 °C				300 °C			
	1	2	3	4	1	2	3	4
4-IPP	27.5	29.5	32.8	35.3	32.4	32.8	36.3	37.0
2-IPP	28.6	28.0	27.9	26.4	25.8	25.9	25.5	23.3
2,4-DIPP	20.4	18.6	15.3	14.5	18.6	16.6	13.8	14.5
2,6-DIPP	15.7	13.0	13.1	12.4	13.3	12.9	12.2	12.1
IPPE	3.9	3.1	3.3	3.1	2.7	3.2	4.1	4.3
Others	3.9	7.8	7.6	8.3	7.2	8.6	8.1	8.8
*Conversion	25.5	32.2	45.8	48.4	37.6	46.4	61.5	62.2
	350 °C				400 °C			
4-IPP	35.0	36.5	38.2	38.8	37.1	38.1	42.3	41.9
2-IPP	22.8	24.7	22.9	21.0	20.9	22.1	20.1	19.1
2,4-DIPP	17.9	14.8	13.6	13.5	15.7	13.3	11.9	10.8
2,6-DIPP	13.7	11.5	12.3	13.0	11.7	9.7	9.4	8.7
IPPE	3.2	3.5	2.7	3.3	4.5	4.4	3.7	4.2
Others	7.4	9.0	10.3	10.4	10.1	12.4	12.6	15.3
*Conversion	47.4	57.5	73.3	76.8	44.5	56.5	67.3	72.1

Note: Feed molar ratio = 1:2, phenol space velocity = 1.1 h^{-1}. 1. Al-MCM-41 (100), 2. Al-MCM-41 (50), 3. Fe-Al-MCM-41 (100), 4. Fe-Al-MCM-41 (50).

show the phenol conversions of 47.4 and 57.5 wt% respectively. It is observed from figure 8 that the activity of Fe-incorporated Al-MCM-41 was found to be always higher than that of pure Al-MCM-41 catalysts at all the temperatures studied. At 350 °C, Fe-Al-MCM-41 with Si/Fe ratio of 100 and 50 show the maximum phenol conversions of 72.3 and 76.8 wt% respectively, which are considerably higher than that over Al-MCM-41 (Si/Al = 100 and 50) catalysts. Also, increasing the iron content in Fe-Al-MCM-41 catalysts leads to an increase in phenol conversion considerably. The observed increase in phenol conversion with increasing incorporated iron content may be due to the additional strong Brønsted acidity generated by iron incorporation as evidenced by acidity measurements. The increase in both Lewis and Brønsted acid sites can be related to the presence of appropriately positioned Lewis acid center with respect to Brønsted acid sites, which may strengthen the acidity of these Brønsted acid sites [28]. Similarly, iron, which itself is a Lewis acid, seems to enhance the overall acidity of the resulting material.

The effect of iron incorporation on the product selectivity can be studied by comparing the product selectivity of Al-MCM-41 and Fe-Al-MCM-41 molecular sieves at a specific reaction condition. Figure 9 shows the product selectivity in phenol isopropylation over Al-MCM-41 (50) and Fe-Al-MCM-41 (50) catalysts at 250 °C. It is observed that the 4-IPP selectivity is found to increase by iron incorporation. Catalyst Fe-Al-MCM-41 (50) shows 35.5% selectivity toward 4-IPP,

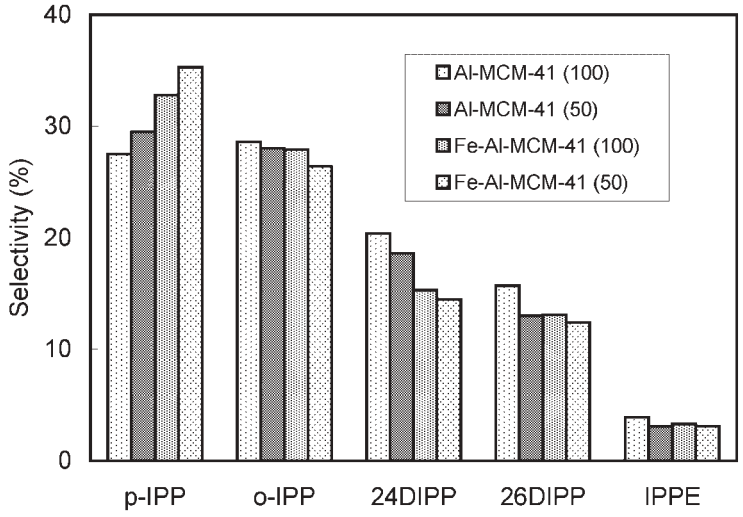

Figure 9. Product selectivity in isopropylation of phenol over different catalysts at 250 °C.

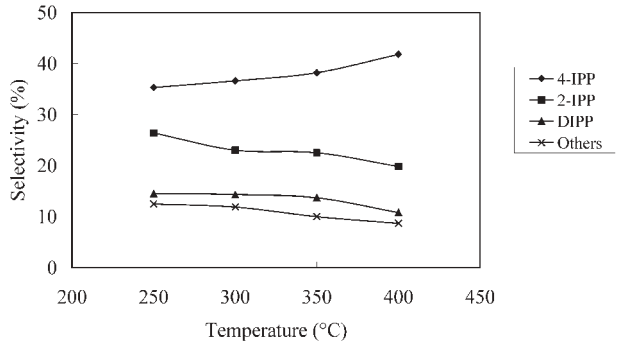

Figure 10. Effect of temperature on the products selectivity over Fe-Al-MCM-41 (50) catalyst.

which is considerably higher than that on Al-MCM-41 (50) at 250 °C. The increase in 4-IPP selectivity by iron incorporation (increasing acidity) may be due to the favoring of *p*-isopropylation by the stronger Brønsted acid sites generated. But the selectivity to 2-IPP is found to decrease with increasing acidity. Also, the selectivity to undesired products was found to be higher over catalysts with strong acidity. The strong Brønsted acid catalysts exhibited a closer proportionality against the activity compared with catalysts with weak acid sites, indicating that the strong Brønsted acid sites are the controlling factor in isopropylation of phenol.

The product distribution in isopropylation of phenol at various temperatures over different catalysts is presented in table 3. The selectivity of various products at different temperatures over the typical catalyst Fe-Al-MCM-41 (50) is presented in figure 10. Generally, when increasing the temperature, the selectivity to 4-IPP and undesired products increased steadily over all the catalytic systems. But the 2-IPP and DIPPs (2,4-DIPP and 2,6-DIPP) selectivity is found to decrease with increasing reaction temperature. The fall in the selectivity of 2-IPP can be accounted by the fact that at higher reaction temperatures, owing to steric hindrance, thermodynamically unfavored ortho isomer (2-IPP) readily isomerized into less-hindered, partially kinetically favorable para isomer (4-IPP). The higher selectivity of 4-IPP at higher temperatures could be due to the absence of secondary alkylation reaction [9,12,20]. The Fe-containing Al-MCM-41 catalysts show comparatively higher selectivity toward 4-IPP and 2-IPP at all the reaction temperatures studied, probably due to the strong Brønsted acid sites generated by iron incorporation in the framework.

The presence of phenolic (-OH) group kinetically favors ortho alkylation [19]. Tanabe and Nishizaki [36] and Klemm *et al.* [37] carried out phenol *t*-butylation and suggested a vertical orientation in the adsorption of phenol molecules at Lewis acid sites, the ortho position of phenol being close to the surface and *t*-butylation at *o*-position occurred predominantly. But the Brønsted acid sites strongly interact with the aromatic ring of the adsorbed phenol, thus bringing it closer to the surface and permitting *t*-butylation in the ortho and para positions. Similarly, in the present case, catalysts with strong Brønsted acid sites are found to enhance the isopropylation at para position, i.e., Fe-Al-MCM-41 (50) shows the maximum *p*-isomer (4-IPP) selectivity among the catalysts studied. In the case of 2-IPP, owing to steric hindrance by bulky isopropyl group in its ortho position, most of the formed 2-IPPs are isomerized into 4-IPP at higher reaction temperatures. Also, owing to the bulky nature of the isopropyl group in ortho position, the *ortho*-IPP (2-IPP) could react with IPA to form 2,4-DIPP and 2,6-DIPP. The selectivity of 2,4-DIPP is more than that of 2,6-DIPP over all the catalytic systems, as the former is thermally more stable than the latter.

The oxygen-alkylated product (IPPE) selectivity is found to decrease with increasing reaction temperature over all the catalytic systems, since the higher temperatures may favor the C-alkylation. Comparatively, Fe-substituted catalysts are found to show lower selectivity to IPPE than that of Al-MCM-41 because the strong Lewis and Brønsted acid sites generated by the

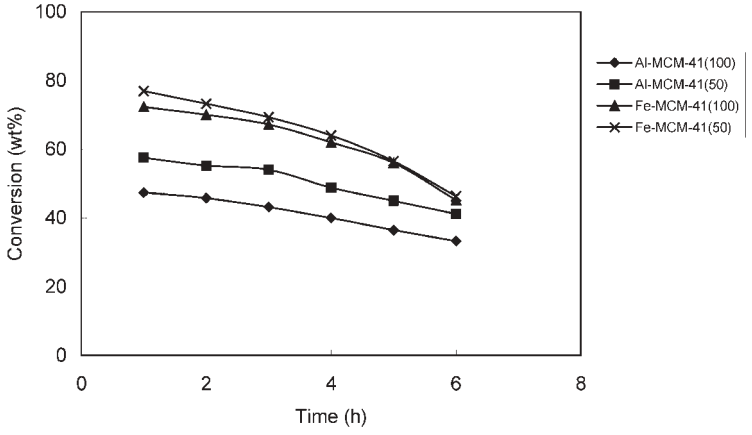

Figure 11. Effect of time onstream in phenol isopropylation over various catalysts at 350 °C.

incorporation of iron in the framework may enhance the C-alkylation.

3.3. Effect of time onstream

The sustainability of the H-form of the above catalysts in phenol isopropylation was studied by carrying out the time onstream study for a duration of 6 h at 350 °C. The optimized feed molar ratio (1 : 2) and phenol flow rate (LHSV = 1.1 h^{-1}) were followed. The phenol conversion obtained over different catalysts during the time onstream study is presented in figure 11. It is found that all the catalysts lose their activity with time. The activity loss is marginal up to a period of 3 h and higher thereafter. Catalysts with strong acid sites deactivate faster than other catalysts. The faster deactivation may be due to higher cracking and coke formation by strong acid sites of the catalysts [38].

4. Conclusions

The low-angle XRD patterns of hydrothermally synthesized Al-MCM-41 and Fe-Al-MCM-41 confirm the hexagonal nature of the materials. The *d*-spacing values of Fe-Al-MCM-41 are found to be higher than that of Al-MCM-41, indicating the incorporation of iron in Al-MCM-41 framework. The nitrogen adsorption studies confirm the mesoporous nature of the materials and the pore diameter and pore volume are found to decrease with increasing metal incorporation. The SEM pictures show that the substituted materials show the formation of aggregates without regular shape. The ^{27}Al MAS NMR spectrum confirms the presence of tetrahedral-coordinated aluminum in the as-synthesized as well as calcined samples. The diffuse reflectance spectra (DRS) characterized by a band around 275 nm, and EPR spectrum with peaks at $g = 4.25$ confirm the presence of Fe (III) ion in the tetrahedral coordination. The acidity measurements by TPD of NH_3 and pyridine-adsorbed FT-IR spectroscopy show that incorporation of iron in Al-MCM-41 framework increases the number of Lewis and Brønsted acid sites. The Fe^{3+} Lewis acid metal may strengthen the appropriately positioned Brønsted acid sites. The isopropylation of phenol with isopropyl acetate over the above catalysts shows that the phenol conversion increases with increasing temperature up to 350 °C and further increase in temperature leads to fall in phenol conversion. The phenol to isopropyl acetate ratio of 1 : 2 and the phenol space velocity of 1.1 h^{-1} are found to be optimum for better phenol conversion as well as 4-IPP selectivity. The activity and selectivity to 4-IPP over Fe-substituted Al-MCM-41 catalysts are always found to be higher than that of the pure Al-MCM-41 catalysts. The higher activities of Fe-substituted materials are due to the strong Brønsted acid sites generated by the strengthening effect of appropriately positioned Lewis acid sites. The time onstream study shows that all the catalysts lose their activity with time, and the strongly acidic catalysts are found to deactivate faster than the other catalysts.

References

[1] A. Knop and L.A. Pilato, *Phenolic Resins Chemistry* (Springer, Berlin, 1985).
[2] M. Inoue and S. Enomoto, Chem. Pharm. Bull. 24 (1976) 2199.
[3] R. Pierantozzi and A.F. Nordquist, Appl. Catal. 21 (1986) 263.
[4] K. Tanabe, T. Nishizaki, G.C. Bond, P.B. Wells and F.C. Tempkins (eds), *Proc. 6th Conf. on Catalysis*, Vol. 11 (The Chemical Society, London, 1977) p. 863.
[5] S. Namba, T. Yashima, Y. Itaba and N. Hara, B. Imelik, C. Naccache, Y. Ben Taarit, J.C. Vedrine, G. Courudier and H. Praliand (eds), *Catalysis by Zeolites* (Elsevier, Amsterdam, 1980) p. 105.
[6] V. Venkat Rao, V. Durga Kumari and S. Narayanan, Appl. Catal. 49 (1989) 165.
[7] R.F. Parton, J.M. Jacobs, H.V. Ootehem and P.A. Jacobs, Stud. Surf. Sci. Catal. 46 (1988) 211.
[8] A. Mitra, Ph.D. Thesis, I.I.T., Bombay (1997) 55.
[9] C.D. Chang and S.D. Hellring, U.S. Patent 5,288,927 (1994).
[10] A. Corma, H. Garcia and J. Primo, J. Chem. Res. (1988) 40.
[11] S. Subramanian, A. Mitra, C.V.V. Satyanarayana and D.K. Chakrabarty, Appl. Catal. A 159 (1997) 229.
[12] K. Zhang, C. Huang, H. Zhang, S. Xiang, S. Liu, D. Xu and H. Li, Appl. Catal. A 166 (1998) 89.
[13] J.W. Yoo, C.W. Lee, B. Wang and S.E. Park, Bull. Korean Chem. Soc. 22(3) (2001) 263.
[14] C.T. Kresge, M.E. Leonowicz, W.J. Roth, J.C. Vartuli and J.S. Beck, Nature 359 (1992) 710.
[15] J.S. Beck, J.C. Vartuli, W.J. Roth, M.E. Leonowicz, C.T. Kresge, K.D. Schmitt, C.T.W. Chu, D.H. Olsen, E.W. Sheppard, S.B. McCullen, J.B. Higgins and J.L. Schlenkar, J. Am. Chem. Soc. 114 (1992) 10835.
[16] R. Ryoo and J.M. Kim, J. Chem. Soc. Chem. Commun. (1995) 711.
[17] Z. Luan, C.F. Cheng, H. He and J. Klinowski, J. Phys. Chem. 99 (1995) 10590.
[18] T. Inui, J.B. Kim and M. Seno, Catal. Lett. 29 (1994) 271.
[19] O. Franke, J. Pathousky, G. Schultz-Ekloff, J. Starek and A. Zukkal, Stud. Surf. Sci. Catal. A 84 (1994) 77.
[20] A. Sakthivel, S.K. Badamali and P. Selvam, Micro. Meso. Mater. 39 (2000) 457.
[21] N. He, S. Bao and Q. Xu, Appl. Catal. A 169 (1998) 29.
[22] S.K. Badamali, A. Sakthivel and P. Selvam, Catal. Lett. 65 (2000) 153.
[23] X.S. Zhao, G.Q. Lu and G.J. Millar, Catal. Lett. 38 (1996) 33.
[24] R.B. Borade and A. Clearfield, Catal. Lett. 31 (1995) 267.
[25] P.J. Branton, P.G. Hall and S.W. Sing, J. Chem. Soc., Faraday Trans. 90 (19) (1994) 2965.
[26] H.B.S. Chan, P.M. Budd and T.deV. Naylor, J. Mater. Chem. 11 (2001) 951.
[27] R. Mokaya and W. Jones, J. Catal. 172 (1997) 211.
[28] K. Chaudhari, T.K. Das, A.J. Chandwadkar and S. Sivasanker, J. Catal. 189 (1999) 81.
[29] B. Echchahed, A. Moen, D. Nicholson and L. Bonneviot, Chem. Mater. 9 (1997) 1716.
[30] Y. Wang, Q. Zhang, T. Shishido and K. Takehira, J. Catal. 209 (2002) 186.
[31] E.G. Derouane, M. Mestsdagh and L. Vielvoye, J. Catal. 33 (1974) 169.

[32] S. Bordiga, R. Buzzoni, F. Geobaldo, C. Lamberti, E. Giamello, A. Zecchina, G. Leofanti, G. Petrini, G. Tozzola and G. Vlaic, J. Catal. 158 (1996) 486.
[33] H. Kosslick, G. Lischke, B. Parlitz, W. Storek and R. Fricke, Appl. Catal. A: Gen. 184 (1999) 49.
[34] R. Mokaya and W. Jones, Chem Commun. (1996) 983.
[35] T.K. Miller and V.H. Grassian, Catal. Lett. 46 (1997) 213.
[36] K. Tanabe and T. Nishizaki, in *Proc. 6th Int. Congress on Catalysis*, F.C. Tompkins (ed.) (The Chemical Society, London, 1977).
[37] L.H. Klemm, C.E. Kloptenstein and J. Shabtar, J. Org. Chem. 35 (1970) 1069.
[38] E. Santaccesaria, D. Grasso, D. Gelosa and S. Carra, Appl. Catal. 64 (1990) 83.